Subwavelength 8 × 8 Butler Matrix With Pixel Metamaterial for Space Limited Systems

Pengyu Fu, Yongjian Zhang, *Member, IEEE*, Mingzhe Hu, *Graduate Student Member, IEEE*, Ziheng Zhou, *Member, IEEE*, Hao Li, and Yue Li, *Senior Member, IEEE*

***Abstract*—In this letter, a subwavelength 8 × 8 Butler matrix (BM) with inverse-designed pixel metamaterial is proposed for space limited systems. With inverse-designed metamaterial, the broadband asymmetric 3-dB couplers with arbitrary phase difference are constructed, which eliminates the space for phase delay lines in BM, significantly reducing the overall size. Finally, a prototype of the proposed BM is fabricated and measured, which exhibits a bandwidth of 21.6% by occupying a compact size of $0.95\lambda_0 \times 0.70\lambda_0 \times 0.01\lambda_0$. With a subwavelength scale, the proposed ultracompact BM can be easily integrated with antenna array for applications in compact multibeam systems.**

***Index Terms*—Butler matrix (BM), couplers, metamaterial, size miniaturization, space limited systems.**

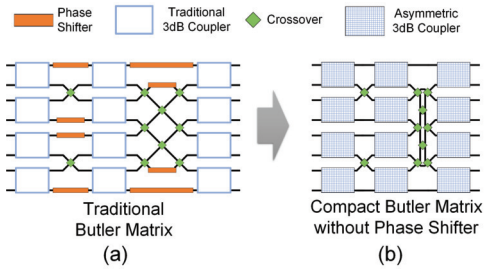

Fig. 1. Strategies for miniaturizing BM. (a) Traditional BM. (b) Compact BM without phase shifters based on asymmetric couplers.

I. Introduction

With the development of wireless communications, multibeam antenna arrays are widely applied in various space limited scenarios [1], [2], [3], [4], offering the advantages of low power consumption and high integration [5], [6], [7]. The feeding networks of antenna array have received extensive attention in recent years. Rotman lens and Luneburg lens realize different phase shifts to the antenna ports in a massive propagation system [8], [9], [10], [11]. In addition, the reflection and transmission arrays based on metasurfaces have been widely studied for multibeam systems [12], [13], [14], [15]. However, these lens-based methods often require multiple wavelength sizes, limiting the integration with antenna arrays [16], [17].

As another method, Butler matrix (BM) has been widely studied as a feeding network with guided wave structures [18], [19], [20], [21], [22], [23], [24], [25]. However, the BM still takes up a much larger area than the antenna array, limiting the further applications in space limited scenarios [26], [27]. Therefore, a number of methods have been proposed for miniaturization of BM. Transmission lines with high impedance and artificial transmission lines are used to reduce the size of BM [28], [29], [30], [31]. What is more, the size of BM can be reduced by decreasing the number of input or output ports but results in a loss of functionality [32]. Specially designed couplers and crossovers are used to reduce the whole footprint, but within the limitation of bandwidth [33], [34], [35], [36], [37].

In this letter, a subwavelength BM with eight input ports and eight output ports is proposed. Based on the pixel metamaterial, asymmetric 3-dB couplers with arbitrary phase difference can be inversely designed. Thus, the phase shifters in the BM can be integrated into couplers, downsizing the overall size of BM. A prototype of the proposed BM is constructed. The measured results show that, at a compact scale of $0.95\lambda_0 \times 0.70\lambda_0 \times 0.01\lambda_0$, an impedance bandwidth of 3.30–4.10 GHz is achieved with high port isolation and output balance. With the merits of subwavelength size and wide bandwidth, the proposed BM can be adapted in multibeam antenna systems for space limited scenarios as mobile terminals, satellites, and radars.

II. Design and Methods

A. Miniaturization Strategy

A conventional BM consists of symmetrical 3-dB couplers, crossovers, and phase shifters. As an example, Fig. 1(a) illustrates the architecture of a BM with eight-port inputs and eight-port outputs. The different lengths of orange lines represent different phase shifters. In addition to the 22.5°, 45°, and 67.5° phase shifts required by the BM structure, these phase shifters must account for the different electrical lengths brought in by the crossovers, which often requires a delay length close to half a wavelength, limiting the integration and bandwidth of the BM. Thus, by utilizing asymmetric 3-dB couplers with arbitrary phase differences at the output ports, the phase shifters in a conventional BM can be shrunk into

Received 23 February 2025; accepted 16 March 2025. Date of publication 1 April 2025; date of current version 9 June 2025. This work was supported in part by the National Key Research and Development Program of China under Grant 2021YFA0716601 and in part by the National Natural Science Foundation of China under Grant U22B2016. *(Corresponding author: Yue Li.)*

Pengyu Fu, Yongjian Zhang, Mingzhe Hu, and Yue Li are with the Department of Electronic Engineering, Beijing National Research Center for Information Science and Technology, Tsinghua University, Beijing 100084, China (e-mail: lyee@tsinghua.edu.cn).

Ziheng Zhou is with the College of Physics and Information Engineering, Fuzhou University, Fuzhou 350108, China (e-mail: zhouzh@fzu.edu.cn).

Hao Li is with the Department of Wireless Technology, Huawei Technology Company Ltd., Shanghai 201206, China (e-mail: lihao485@huawei.com).

Digital Object Identifier 10.1109/LMWT.2025.3552854

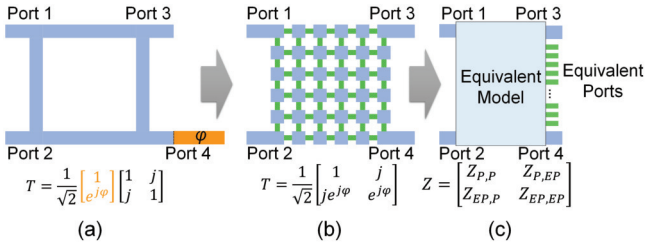

Fig. 2. Design of asymmetric couplers. (a) Traditional 3-dB couplers. (b) Asymmetric couplers based on metamaterial. (c) Equivalent circuit model.

the couplers, reducing the overall length of the BM, shown in Fig. 1(b).

B. Inverse-Designed Asymmetric 3-dB Coupler

The conventional 3-dB couplers are designed with a symmetrical structure, as shown in Fig. 2(a). However, in BM, there is always a phase shifter connected after one of the output ports. With pixel metamaterial, asymmetric couplers can be inversely designed without adding extra area. The basic architecture of the proposed pixel metamaterial is illustrated in Fig. 2(b). Several square pixel-like patches are filled between the four ports. Different structures can be constructed by controlling the ON/OFF states of the sticks between patches, realizing different four-port network functions. The proposed pixel metamaterial can be further analyzed by an equivalent circuit model, as shown in Fig. 2(b) and (c). The whole base unit of pixel metamaterial can be regarded as a circuit model with four feeding ports and N internal equivalent ports. The internal equivalent ports are used to represent whether the sticks between patches are connected. Specifically, the impedance value of the equivalent port can be set to 0 for short-circuit or ∞ for open-circuit, representing the ON/OFF states of the linking sticks, and the impedance of equivalent ports can be organized into a diagonal matrix Z_{EP}, with a total of 2^N possible values

$$Z_{\mathrm{EP}} = \mathrm{diag}\left(Z_{\mathrm{EP}}^1, Z_{\mathrm{EP}}^2, \ldots, Z_{\mathrm{EP}}^N\right). \tag{1}$$

Then, the impedance characteristics of four-port network Z_{P} can be derived from the impedance matrix Z of the $N+4$ ports and the matrix Z_{EP} of the equivalent ports

$$Z = \begin{bmatrix} Z_{\mathrm{P,P}} & Z_{\mathrm{P,EP}} \\ Z_{\mathrm{EP,P}} & Z_{\mathrm{EP,EP}} \end{bmatrix} \tag{2}$$

$$\begin{bmatrix} V_{\mathrm{P}} \\ V_{\mathrm{EP}} \end{bmatrix} = \begin{bmatrix} Z_{\mathrm{P,P}} & Z_{\mathrm{P,EP}} \\ Z_{\mathrm{EP,P}} & Z_{\mathrm{EP,EP}} \end{bmatrix} \begin{bmatrix} I_{\mathrm{P}} \\ I_{\mathrm{EP}} \end{bmatrix} \tag{3}$$

$$V_{\mathrm{EP}} = Z_{\mathrm{EP}} I_{\mathrm{EP}} \tag{4}$$

$$Z_{\mathrm{P}} = Z_{\mathrm{P,P}} + Z_{\mathrm{P,EP}}(Z_{\mathrm{EP}} - Z_{\mathrm{EP,EP}})^{-1} Z_{\mathrm{EP,P}} \tag{5}$$

and the transfer function of this four-port network T can be further calculated from Z_{P}, offering the possibility to quickly get the electromagnetic functions of different states of sticks.

The inverse design process can be divided into the several steps, as shown in Fig. 3. First, the basic structure of the pixel metamaterial is designed. Second, the phase design target for the asymmetric coupler is determined. Finally, the genetic algorithm is employed to minimize the loss function for the specified design targets. The loss function is set as

$$L = \sum_{\omega} \left(k_p L_p(\varphi, \omega) + k_a L_a(\omega)\right) \tag{6}$$

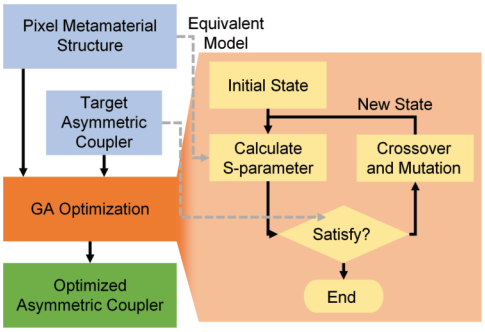

Fig. 3. Design flowchart of asymmetric couplers.

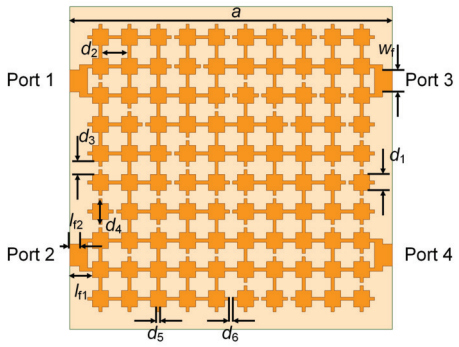

Fig. 4. Structure parameters of pixel metamaterial. a = 20, w_{f} = 1.37, l_{f1} = 1.4, l_{f2} = 0.6, d_1 = 1, d_2 = 1.6, d_3 = 0.8, d_4 = 1.6, d_5 = 0.2, and d_6 = 0.2 mm.

where L_a and L_p represent the term related to the transmission amplitude and phase, respectively. Starting from a random set of states, the equivalent circuit model is utilized to rapidly calculate the S-parameters of different structures. The crossover and mutation process are used to generate new state for optimization until the target is satisfied.

As an example, shown in Fig. 4, a pixel metamaterial is illustrated to optimize an asymmetric 3-dB coupler, which consists of 10 × 10 patches and four feeding ports. The dimensions of the whole structure are selected close to a conventional 3-dB coupler. The selection of the patch number and the structure dimensions considers factors such as mutual constraint between optimization accuracy and size and computational complexity. The optimization results indicate that, within the wide frequency range of 3.3–3.8 GHz, asymmetric 3-dB couplers with minimal phase error can be achieved when the required additional phase difference is less than 90°, thereby fulfilling the design criteria for compact BM.

III. BM Design

Based on the above asymmetric 3-dB couplers with arbitrary phase differences, a compact 8 × 8 BM model is designed and depicted in Fig. 5. Two crossover sections are designed and simulated to determine the required phase delay. According to the structure of BM and crossover sections, five different asymmetric 3-dB couplers with different phase responses are required, marked as A-E in Fig. 5(a). Specifically, the asymmetric couplers from A to E are required to be inversely designed with additional phase differences of 57.4°, 42.9°, 67.2°, 31.2°, and 67.8° at central frequency point.

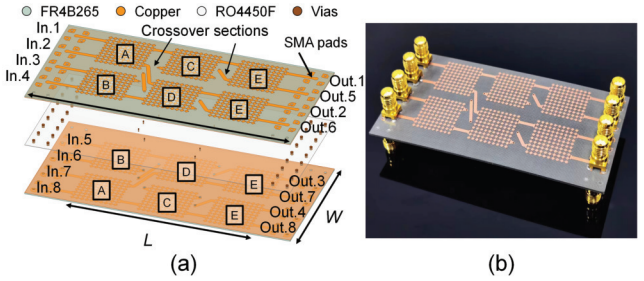

Fig. 5. Structure of BM. (a) Multilayer structure and (b) prototype of BM.

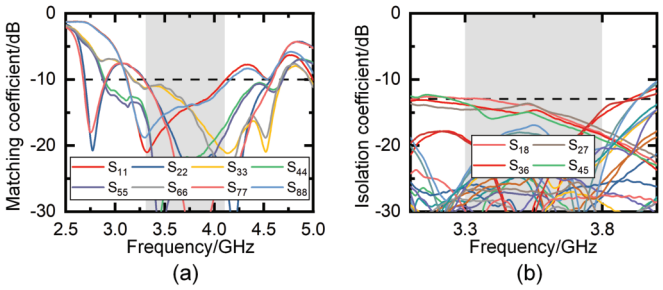

Fig. 6. Measured *S*-parameters results of BM. (a) Matching coefficient of each input ports. (b) Isolation between the input ports of the BM.

TABLE I
PERFORMANCE COMPARISON

Ref.	I.O.	IL (dB)	PI (°)	AI (dB)	Iso. (dB)	Area (λ_0^2)	BW (%)	BW/Area (%/λ_0^2)
[25]	8×8	1.9	12	0.7	19	1.6×1.2	5.5	0.029
[35]	4×4	1.5*	35*	1.5*	10	2.7×2.2	13.6	0.023
[36]	4×4	2.0	33*	3*	16.5	2.1×2.0	5.3	0.013
[38]	9×9	2.19	16.2	1.2	15	4.3×8.1	6.9	0.002
[39]	4×4	0.6	8	1.4	14	3.5×2.2	13.8	0.018
[40]	4×4	1.8	13	1.8	12	2.3×1.4	33.3	0.103
[41]	4×4	1.2	36	1.5	17	9.0×2.9*	15.4	0.006
[42]	5×5	1.2	8.3	2.5*	NG	10.4×2.9	3.75	0.001
Com.	8×8	3.0	12	3	12	3.1×2.7	100	0.112
This work	**8×8**	**1.9**	**25**	**2.2**	**13**	**0.95×0.7**	**21.6**	**0.325**

I.O.: Input and output ports; IL: Insertion Loss; PI: Phase Imbalance; AI: Amplitude Imbalance; Iso.: Isolation; BW: Bandwidth; λ_0: Free space wavelength at central frequency; NG: Not Given. Com.: Commercial BM (by MICABLE with model SA-07-8B020060, 2-6 GHz)
* Estimate from the figures in reference.

Combining the inverse-designed asymmetric couplers and crossover sections, the BM is composed of two identical single-layer FR4B265 boards (ε_r = 2.65 and tanθ = 0.002) with a thickness of 0.508 mm, which are joined together by RO4450F prepreg (ε_r = 3.52 and tanθ = 0.004) with a thickness of 0.1 mm. The BM is fed through 16 surface-mounted 50-Ω subminiature version A (SMA) connectors, and the metallic vias represented by the brown portion are used for the electrical connection of the upper and lower layers, as well as the connection of the SMA connectors to the microstrip lines.

IV. EXPERIMENTAL RESULTS

As shown in Fig. 5(b), a prototype of the proposed BM is constructed, occupying an overall size of 70 × 50 × 1.116 mm^3 without feeding structures. The 16 SMA connectors are soldered to the BM for 50-Ω coaxial feeding

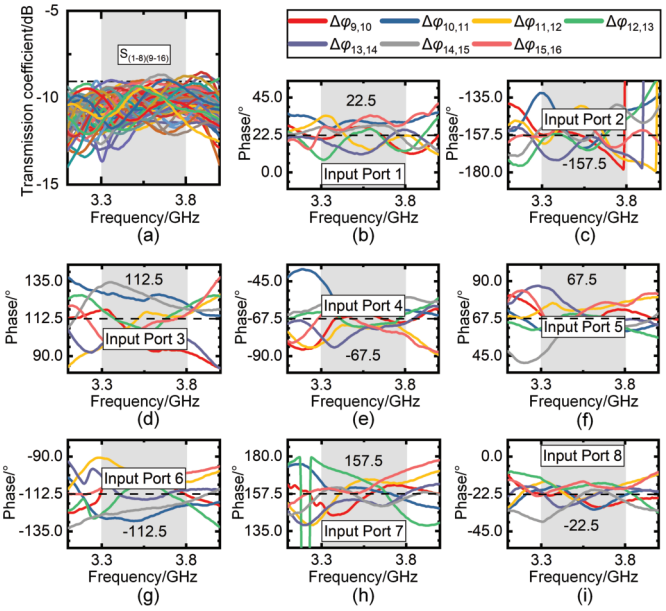

Fig. 7. Measured transmission coefficient. (a) Transmission amplitude. (b)–(i) Transmission phase gradient with an input port from 1 to 8.

lines, and the performance of this BM is measured with the N9917A vector network analyzer. Fig. 6 depicts the measured *S*-parameters of the propounded BM. The measured −10-dB impedance bandwidth is 3.30–4.10 GHz. Meanwhile, the isolation between each input port of the BM is higher than 13 dB in the 3.30–3.80-GHz frequency band for 5G communications, which can satisfy the application requirements of the mobile terminals, as shown in Fig. 6(b). In addition, Fig. 7(a) demonstrates the *S*-parameters from eight different input ports to eight different output ports, indicating an insertion loss with 1.9 dB and amplitude imbalance of 2.2 dB in the 3.3–3.8-GHz frequency band. What is more, Fig. 7(b)–(i) depicts the measured phase gradient formed at the output ports from each input ports. From ports 1 to 8, different phase gradient differences of 22.5°, −157.5°, 112.5°, −67.5°, 67.5°, −112.5°, 157.5°, and −22.5° are formed at the output ports in the frequency bandwidth, with a phase imbalance of 25°. Table I lists the performance comparisons between the proposed BM and other recent existing designs. Compared with previous designs, with comparable insertion loss and output imbalance, the proposed compact BM based on inverse-designed pixel metamaterials achieves subwavelength scale and greatly improves the ratio of bandwidth to footprint.

V. CONCLUSION

As a conclusion, in this article, a subwavelength 8 × 8 BM is proposed for integrated multibeam antenna arrays. Based on inverse-designed metamaterial, asymmetric 3-dB couplers with arbitrary phase difference can be customized, which obviates the phase shifters in BM and reduces its overall footprint. The measured results indicate that the proposed BM exhibits a bandwidth of 21.6% within a subwavelength scale. At the same time, the methodology of pixel metamaterial is adaptable to other integrated BM, exhibiting a promising potential for on-chip multibeam antennas in mobile terminals, satellites, radars, and such type of space limited systems.

REFERENCES

[1] W. Hong et al., "Multibeam antenna technologies for 5G wireless communications," *IEEE Trans. Antennas Propag.*, vol. 65, no. 12, pp. 6231–6249, Dec. 2017.

[2] B. Palacin et al., "Multibeam antennas for very high throughput satellites in Europe: Technologies and trends," in *Proc. 11th Eur. Conf. Antennas Propag. (EUCAP)*, Paris, France, May 2017, pp. 2413–2417.

[3] W. Menzel and A. Moebius, "Antenna concepts for millimeter-wave automotive radar sensors," *Proc. IEEE*, vol. 100, no. 7, pp. 2372–2379, Jul. 2012.

[4] H. Li, Y. Li, L. Chang, W. Sun, X. Qin, and H. Wang, "A wideband dual-polarized endfire antenna array with overlapped apertures and small clearance for 5G millimeter-wave applications," *IEEE Trans. Antennas Propag.*, vol. 69, no. 2, pp. 815–824, Feb. 2021.

[5] R. Lu, C. Yu, Y. Zhu, and W. Hong, "Compact millimeter-wave endfire dual-polarized antenna array for low-cost multibeam applications," *IEEE Antennas Wireless Propag. Lett.*, vol. 19, no. 12, pp. 2526–2530, Dec. 2020.

[6] Y. M. Cheng, P. Chen, W. Hong, T. Djerafi, and K. Wu, "Substrate-integrated-waveguide beamforming networks and multibeam antenna arrays for low-cost satellite and mobile systems," *IEEE Antennas Propag. Mag.*, vol. 53, no. 6, pp. 18–30, Dec. 2011.

[7] P. Fu, Y. Zhang, M. Hu, Z. Chen, P. Liu, and Y. Li, "A low-power-consumption massive MIMO scheme based on multibeam antenna array," *Microw. Opt. Technol. Lett.*, vol. 64, no. 8, pp. 1428–1433, Aug. 2022.

[8] W. Rotman and R. Turner, "Wide-angle microwave lens for line source applications," *IEEE Trans. Antennas Propag.*, vol. AP-11, no. 6, pp. 623–632, Nov. 1963.

[9] S. Vashist, M. K. Soni, and P. K. Singhal, "A review on the development of Rotman lens antenna," *Chin. J. Eng.*, vol. 2014, pp. 1–9, Jul. 2014.

[10] R. K. Luneburg, *Mathematical Theory of Optics*. Berkeley, CA, USA: Univ. California Press, 1966.

[11] L. C. Gunderson and G. T. Holmes, "Microwave Luneburg lens," *Appl. Opt.*, vol. 7, no. 5, p. 801, 1968.

[12] D. González-Ovejero, G. Minatti, G. Chattopadhyay, and S. Maci, "Multibeam by metasurface antennas," *IEEE Trans. Antennas Propag.*, vol. 65, no. 6, pp. 2923–2930, Jun. 2017.

[13] H.-X. Xu, T. Cai, Y.-Q. Zhuang, Q. Peng, G.-M. Wang, and J.-G. Liang, "Dual-mode transmissive metasurface and its applications in multibeam transmitarray," *IEEE Trans. Antennas Propag.*, vol. 65, no. 4, pp. 1797–1806, Apr. 2017.

[14] S. Yin, E. Galiffi, and A. Alù, "Floquet metamaterials," *eLight*, vol. 2, no. 1, pp. 1–13, May 2022.

[15] L. Li, H. Zhao, C. Liu, L. Li, and T. J. Cui, "Intelligent metasurfaces: Control, communication and computing," *eLight*, vol. 2, no. 1, p. 7, May 2022.

[16] H. Li, Z. Zhou, Y. Zhao, and Y. Li, "Low-loss beam synthesizing network based on Epsilon-near-zero (ENZ) medium for on-chip antenna array," *Chip*, vol. 2, no. 2, Jun. 2023, Art. no. 100049.

[17] W. Sun, Y. Li, L. Chang, H. Li, X. Qin, and H. Wang, "Dual-band dual-polarized microstrip antenna array using double-layer gridded patches for 5G millimeter-wave applications," *IEEE Trans. Antennas Propag.*, vol. 69, no. 10, pp. 6489–6499, Oct. 2021.

[18] J. Butler and R. Lowe, "Beam-forming matrix simplifies design of electronically scanned antennas," *Electron. Des.*, vol. 9, pp. 170–173, Apr. 1961.

[19] A. K. Vallappil, M. K. A. Rahim, B. A. Khawaja, N. A. Murad, and M. G. Mustapha, "Butler matrix based beamforming networks for phased array antenna systems: A comprehensive review and future directions for 5G applications," *IEEE Access*, vol. 9, pp. 3970–3987, 2021.

[20] M. Bona, L. Manholm, J. P. Starski, and B. Svensson, "Low-loss compact Butler matrix for a microstrip antenna," *IEEE Trans. Microw. Theory Techn.*, vol. 50, no. 9, pp. 2069–2075, Sep. 2002.

[21] J.-S. Néron and G.-Y. Delisle, "Microstrip EHF Butler matrix design and realization," *ETRI J.*, vol. 27, no. 6, pp. 788–797, Dec. 2005.

[22] Q.-L. Yang, Y.-L. Ban, J.-W. Lian, Z.-F. Yu, and B. Wu, "SIW Butler matrix with modified hybrid coupler for slot antenna array," *IEEE Access*, vol. 4, pp. 9561–9569, 2016.

[23] J. Remez and R. Carmon, "Compact designs of waveguide Butler matrices," *IEEE Antennas Wireless Propag. Lett.*, vol. 5, pp. 27–31, 2006.

[24] M. Nedil, T. A. Denidni, and L. Talbi, "Novel Butler matrix using CPW multilayer technology," *IEEE Trans. Microw. Theory Techn.*, vol. 54, no. 1, pp. 499–507, Jan. 2006.

[25] Q. Shao, F.-C. Chen, Y. Wang, and Q.-X. Chu, "Design of 4 × 4 and 8 × 8 filtering Butler matrices utilizing combined 90° and 180° couplers," *IEEE Trans. Microw. Theory Techn.*, vol. 69, no. 8, pp. 3842–3852, Aug. 2021.

[26] Y. Zhang, Y. Li, W. Zhang, Z. Zhang, and Z. Feng, "Omnidirectional antenna diversity system for high-speed onboard communication," *Engineering*, vol. 11, pp. 72–79, Apr. 2022.

[27] Y. Zhang and Y. Li, "Wideband microstrip antenna in small volume without using fundamental mode," *Electromagn. Sci.*, vol. 1, no. 2, pp. 1–6, Jun. 2023.

[28] C.-H. Tseng, C.-J. Chen, and T.-H. Chu, "A low-cost 60-GHz switched-beam patch antenna array with Butler matrix network," *IEEE Antennas Wireless Propag. Lett.*, vol. 7, pp. 432–435, 2008.

[29] C.-W. Wang, T.-G. Ma, and C.-F. Yang, "A new planar artificial transmission line and its applications to a miniaturized Butler matrix," *IEEE Trans. Microw. Theory Techn.*, vol. 55, no. 12, pp. 2792–2801, Dec. 2007.

[30] K. Wincza, S. Gruszczynski, and K. Sachse, "Broadband planar fully integrated 8 × 8 Butler matrix using coupled-line directional couplers," *IEEE Trans. Microw. Theory Techn.*, vol. 59, no. 10, pp. 2441–2446, Oct. 2011.

[31] Y. S. Jeong and T. W. Kim, "Design and analysis of swapped port coupler and its application in a miniaturized Butler matrix," *IEEE Trans. Microw. Theory Techn.*, vol. 58, no. 4, pp. 764–770, Apr. 2010.

[32] Y. Zhang and Y. Li, "A dimension-reduction multibeam antenna scheme with dual integrated Butler matrix networks for low-complex massive MIMO systems," *IEEE Antennas Wireless Propag. Lett.*, vol. 19, no. 11, pp. 1938–1942, Nov. 2020.

[33] S. A. Babale, S. K. A. Rahim, O. A. Barro, M. Himdi, and M. Khalily, "Single layered 4 × 4 Butler matrix without phase-shifters and crossovers," *IEEE Access*, vol. 6, pp. 77289–77298, 2018.

[34] G. Tian, J. Yang, and W. Wu, "A novel compact Butler matrix without phase shifter," *IEEE Microw. Wireless Compon. Lett.*, vol. 24, no. 5, pp. 306–308, May 2014.

[35] M. K. Ishfaq et al., "Compact wide-angle scanning multibeam antenna array for V2X communications," *IEEE Antennas Wireless Propag. Lett.*, vol. 20, pp. 2141–2145, 2021.

[36] S. Tang, Y. Zhang, J. Rao, Z. Han, C.-Y. Chiu, and R. Murch, "Beamforming network design utilizing node microstrip architectures for dual-polarized endfire millimeter-wave antenna arrays," *IEEE Trans. Antennas Propag.*, vol. 71, no. 6, pp. 4862–4873, Jun. 2023.

[37] M.-Y. Huang, T.-Y. Huang, M. Swaminathan, and H. Wang, "Concurrent multi-directional beam-forming receiving network for full-FoV high-efficiency wireless power transfer," in *IEEE MTT-S Int. Microw. Symp. Dig.*, Boston, MA, USA, Jun. 2019, pp. 1511–1514.

[38] C. Geng, J.-W. Lian, Y. J. Guo, and D. Ding, "Millimeter-wave three-layer substrate-integrated 9 × 9 Butler matrix and its application to wide-angle endfire multibeam metasurface antenna," *IEEE Trans. Microw. Theory Techn.*, vol. 72, no. 4, pp. 2253–2266, Feb. 2024.

[39] M. O. Shady and A. A. Kishk, "Compact 4 × 4 multilayer Butler matrix with four-slot array," *IEEE Trans. Microw. Theory Techn.*, vol. 72, no. 6, pp. 3522–3529, Jun. 2024.

[40] X.-Z. Wang, F.-C. Chen, and Q.-X. Chu, "A compact broadband 4 × 4 Butler matrix with 360° continuous progressive phase shift," *IEEE Trans. Microw. Theory Techn.*, vol. 71, no. 9, pp. 3906–3914, Sep. 2023.

[41] D. Cao, Y. Li, and J. Wang, "Ka-band multibeam patch antenna array fed by spoof-surface-plasmon-polariton Butler matrix," *IEEE Trans. Antennas Propag.*, vol. 71, no. 3, pp. 2385–2395, Mar. 2023.

[42] B.-Y. Han, X.-Y. Chen, J.-D. Zhang, W. Wu, J.-Y. Zhang, and D.-G. Fang, "General optimized design of the E-plane waveguide Butler matrix with non-2 n beams based on the FFT," *IEEE Trans. Antennas Propag.*, vol. 73, no. 3, pp. 1461–1470, Mar. 2025, doi: 10.1109/TAP.2024.3511933.